All-optical NAND/NOT/AND/OR logic gates based on combined Brillouin gain and loss in an optical fiber

Daisy Williams,* Xiaoyi Bao, and Liang Chen

Department of Physics, University of Ottawa, MacDonald Hall, 150 Louis Pasteur, Ottawa, Ontario K1N 6N5, Canada

*Corresponding author: dwill087@uottawa.ca

Received 9 October 2012; revised 27 March 2013; accepted 5 April 2013;
posted 16 April 2013 (Doc. ID 177737); published 10 May 2013

A combined Brillouin gain and loss process has been proposed in a polarization maintaining optical fiber to realize all-optical NAND/NOT/AND/OR logic gates in the frequency domain. A model describing the interaction of a Stokes, anti-Stokes, and continuous wave and two acoustic waves inside a fiber, ranging in length from 350–2300 m, was used to theoretically model the gates. Through the optimization of the pump depletion and gain saturation in the combined gain and loss process, switching contrasts of 20%–83% have been simulated for different configurations. © 2013 Optical Society of America

OCIS codes: (200.4660) Optical logic; (060.2310) Fiber optics; (190.4370) Nonlinear optics, fibers; (190.5890) Scattering, stimulated; (200.0200) Optics in computing.

http://dx.doi.org/10.1364/AO.52.003404

1. Introduction

In recent years, photonic computing has received considerable attention due to its numerous applications, such as high-speed optical signal processing, which would yield much fast computing times and higher bandwidths. For this reason, optical logic has been the focus of many research efforts and several schemes to improve conventional logic gates have been proposed. In [1–3] optically programmable, and reversible, Boolean logic units are proposed, consisting of a circuit, which is designed by the implementation of a 2×2 optoelectronic switch [4]. The drawback of this scheme is that the switching speed of the 2×2 switching element is about 10^6 times slower compared to, for example, a semiconductor optical amplifier (SOA)-based interferometric switch. In view of the speed limitations inherent in electronic circuits, all-optical data processing devices have become the focus of many research efforts, especially in optical fibers, as these devices provide compatibility to fiber links with low connection loss and easy implementation. One category of such devices is the all-optical logic gate, which is projected to be a main component in future integrated photonic circuits.

Some established techniques for achieving functional all-optical logic gates include the use of integrated optical and waveguide structure Mach–Zehnder interferometers (MZIs) [5–7] that are often limited by back-reflections of the optical signal, which are minimized by extending the cladding and substrate layers; the use of nonlinear optical processes in SOAs, such as four-wave mixing [8] and cross-gain modulation [9–11]; and the use of a combination thereof—integrated MZIs based on SOA [12–15]. SOA-based techniques are often limited by the carrier's recovery time, which in turn slows down the operation of the device. In addition, these techniques often require the use of multiple SOAs to achieve functional all-optical logic gates, and fall victim to additional noise, such as spontaneous emission noise [16,17], time dependent modulation due to time jitter, and birefringence induced signal distortion.

1559-128X/13/143404-08$15.00/0

Additionally, there exist logic gates proposed by terahertz optical asymmetric demultiplexer (TOAD)-based switches [18–21]. The TOAD consists of a loop mirror and a nonlinear element, usually an SOA, which is positioned asymmetrically in the fiber loop. In addition to the limitations of the SOA mentioned above, the TOAD scheme suffers from a walk-off problem due to dispersion, intensity losses due to beam splitter, optical circulators, etc. In addition, if there is an attempt to remedy the aforementioned finite propagation time of the pulse across the SOA by decreasing the offset length, the decrease in effective SOA length causes a reduction in contrast ratio of the TOAD switching mechanism, which hinders the functionality of the logic gate.

Techniques based on the design of simple passive optical components also exist. These techniques include optical logic parallel processors [22] and the multi-output polarization-encoded optical shadow-casting scheme [23]. Both schemes are based on the polarization of light, whereby the switching mechanism consists of the polarization switching of output light. Drawbacks of such schemes include polarization instability, inherent in any polarization-dependent device, and detrimental diffraction effects.

Other such techniques also exist, such as using a Kerr nonlinear prism to realize binary-to-gray-to-binary code conversion, whereby the switching mechanism is the deviation of light due to nonlinear refraction [24]. However, to function correctly, such a scheme requires several such prisms and mirrors to be aligned in series, the configuration of which is both bulky and requires extensive calibration. In addition, very large intensities are required for the function of the proposed setup.

Fiber nonlinearity-based techniques provide comparable functionality, without the limitations mentioned above. Among fiber nonlinearity-based logic gates, one of the techniques includes using the Kerr effect in highly nonlinear fibers to induce birefringence, thereby rotating the polarization state of an output light wave [25,26], which represents the optical gate operation with ultimate speed limitation above 100 Gb/s. However, one limitation of this technique is that long fiber lengths introduce polarization instabilities in conventional single mode fibers. A relatively short fiber length of 2 km was used to realize the XOR gate in [25]. Since polarization rotation is necessary in [25,26], the presence of birefringence is another limitation of the technique, which may cause polarization mode dispersion (PMD) of the optical signal.

Therefore, there is a need for a polarization-independent technique to accurately realize all-optical logic gates, which could be realized in the frequency domain through the combined Brillouin gain and loss spectrum. Polarization maintaining fibers (PMFs) help to eliminate the influence of PMD [27], as well as other polarization maintaining applications [28,29]. Using PMFs ensures that the technique based on combined Brillouin gain and loss is free of polarization induced signal fluctuations at different positions, which causes spectral distortion.

In this paper, a fiber nonlinearity-based technique is proposed to realize all-optical NAND/NOT/AND/OR logic gates, based on the principles of a combined Brillouin gain and loss process in a PMF. Combined Brillouin gain and loss is often advantageous over Brillouin gain in the construction of all-optical gates since it describes the energy transfer between three optical waves, as compared to only two optical waves. Additionally, the combination of simultaneous gain and loss acts to improve the signal-to-noise ratio by approximately twofold [30] upon measurement of the Brillouin gain spectrum. This increases the clarity of signal, as well as the switching contrast in the proposed logic gates. Additionally, the combined gain and loss scheme is more compact than the traditional Brillouin optical correlation-domain analysis system [31,32], which employs successive utilization of the Brillouin gain and loss. The additional parameters in the three-wave interaction give combinations of input powers such that the output signals yield results that correspond to the truth tables of, for example, a NAND gate. The combined Brillouin gain and loss model was used to create several configurations of a functional NAND gate, and a NOT gate. With Brillouin gain one can construct a simplified NOT gate. The combination of the NAND and NOT gates has been used to further construct several configurations of AND and OR gates. Switching contrasts are simulated to be between 20%–83% for various configurations.

2. Model

The process of SBS has been studied in a single mode optical fiber, with core radius of 4.1 μm and power penalty of 0.67 dB/km. The configuration is composed of a continuous wave (CW) launched into one end, and a Stokes wave (SW) and an anti-Stokes wave (ASW) launched into the other end. The schematic arrangement is shown on Fig. 1 below.

The system is deemed to operate in the steady-state regime with pulse lengths greater than the phonon relaxation time, in this case 10 ns [33]. In the slowly varying amplitude approximation, the steady state interaction between the CW, SW, ASW, and two acoustic waves (AW_1 and AW_2), as shown in Fig. 1, is described by the following system of equations [34,35]:

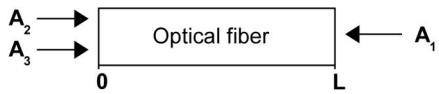

Fig. 1. Schematic arrangement of SBS in a PMF of length L CW and pulse configuration: A_1—continuous wave, A_2—Stokes wave, A_3—anti-Stokes wave.

$$-\frac{dA_1}{dz} = \frac{i\omega_1\gamma_e}{2nc\rho_0}\rho_1 A_2 + \frac{i\omega_1\gamma_e}{2nc\rho_0}\rho_2^* A_3 - \frac{1}{2}\alpha A_1, \quad (1.1)$$

$$\frac{dA_2}{dz} = \frac{i\omega_2\gamma_e}{2nc\rho_0}\rho_1^* A_1 - \frac{1}{2}\alpha A_2, \quad (1.2)$$

$$\frac{dA_3}{dz} = \frac{i\omega_3\gamma_e}{2nc\rho_0}\rho_2 A_1 - \frac{1}{2}\alpha A_3, \quad (1.3)$$

$$(\Omega_B^2 - \Omega_1^2 - i\Omega_1\Gamma_B)\rho_1 = \frac{\gamma_e q_1^2}{4\pi} A_1 A_2^*, \quad (1.4)$$

$$(\Omega_B^2 - \Omega_2^2 - i\Omega_2\Gamma_B)\rho_2 = \frac{\gamma_e q_2^2}{4\pi} A_3 A_1^*, \quad (1.5)$$

where $\Omega_1 = \omega_1 - \omega_2$, $\Omega_2 = \omega_3 - \omega_1$, Ω_1 is the angular frequency of the AW_1 caused by the interaction of CW and SW, Ω_2 is the angular frequency of the AW_2 caused by interaction of CW and ASW, A_1 is the complex amplitude of the CW, A_2 is the complex amplitude of the SW, A_3 is the complex amplitude of the ASW, ρ_1 is the complex amplitude of the AW_1 caused by interaction of CW and SW, ρ_2 is the complex amplitude of the AW_2 caused by interaction of CW and ASW, c is the speed of light, ρ_0 is the density of the fiber, γ_e is the electrostrictive constant, z is the coordinate along the fiber, n is the index of refraction of the fiber, v is the speed of sound in the fiber, Γ_B is the Brillouin linewidth, and Ω_B is the Brillouin frequency defined as $\Omega_B = 2nv\omega_1/c$, where ω_1 is the angular frequency of the CW, ω_2 is the angular frequency of the SW, and ω_3 is the angular frequency of the ASW.

For a two-wave configuration describing Brillouin gain, the ASW terms are simply set to "0" in the following analysis. In the above arrangement, the SW and ASW input parameters are known only at the beginning of the fiber, i.e., at $z = 0$. Correspondingly, the CW input parameters are known only at the end of the fiber, i.e., at $z = L$, where L is the length of the fiber. Therefore, the boundary conditions for system (1) are similar to previously studied configurations with one pulse [33,36]. The conditions for two pulses are as follows:

$$|A_1(L)|^2 = A_{10}^2; \qquad |A_2(0)|^2 = A_{20}^2 \qquad |A_3(0)|^2 = A_{30}^2, \quad (2)$$

where A_{10}^2, A_{20}^2, and A_{30}^2 are known squared absolute values of the complex amplitudes A_1, A_2, and A_3, respectively. In the dimensionless notation, the system (1) becomes

$$\frac{dY_1}{dl} = \beta_1 Y_1 Y_2 - \beta_2 Y_1 Y_3 + \varepsilon Y_1, \quad (3.1)$$

$$\frac{dY_2}{dl} = \beta_3 Y_1 Y_2 - \varepsilon Y_2, \quad (3.2)$$

$$\frac{dY_3}{dl} = -\beta_4 Y_1 Y_3 - \varepsilon Y_3, \quad (3.3)$$

$$Y_4 = \beta_5 Y_1 Y_2, \quad (3.4)$$

$$Y_5 = \beta_6 Y_1 Y_3, \quad (3.5)$$

with corresponding boundary conditions

$$Y_1(1) = 1; \qquad Y_2(0) = 1; \qquad Y_3(0) = 1. \quad (4)$$

The dimensionless variables $l = z/L$, $Y_1 = P_1/P_{10}$, $Y_2 = P_2/P_{20}$, $Y_3 = P_3/P_{30}$, $Y_4 = |\rho_1/\rho_0|^2$, and $Y_5 = |\rho_2/\rho_0|^2$,$\varepsilon = \alpha L$ have been introduced to derive the system (3), as well as the following β-coefficients:

$$\beta_1 = \frac{2\gamma_e^2 k^3 L P_{20}}{\pi r^2 n^3 c\rho_0 \Omega_1 \Gamma_B} \cdot \frac{1}{1+\xi_1^2}, \quad (5.1)$$

$$\beta_2 = \frac{2\gamma_e^2 k^3 L P_{30}}{\pi r^2 n^3 c\rho_0 \Omega_2 \Gamma_B} \cdot \frac{1}{1+\xi_2^2}, \quad (5.2)$$

$$\beta_3 = \frac{2\gamma_e^2 k^3 L P_{10}}{\pi r^2 n^3 c\rho_0 \Omega_1 \Gamma_B} \cdot \frac{1}{1+\xi_1^2}, \quad (5.3)$$

$$\beta_4 = \frac{2\gamma_e^2 k^3 L P_{10}}{\pi r^2 n^3 c\rho_0 \Omega_2 \Gamma_B} \cdot \frac{1}{1+\xi_2^2}, \quad (5.4)$$

$$\beta_5 = \left(\frac{2\gamma_e k^2}{\pi r^2 nc\rho_0 \Omega_1 \Gamma_B}\right)^2 \cdot \frac{1}{1+\xi_1^2} \cdot P_{10} P_{20}, \quad (5.5)$$

$$\beta_6 = \left(\frac{2\gamma_e k^2}{\pi r^2 nc\rho_0 \Omega_2 \Gamma_B}\right)^2 \cdot \frac{1}{1+\xi_2^2} \cdot P_{10} P_{30}, \quad (5.6)$$

$$\xi_1 = \frac{\Omega_B^2 - \Omega_1^2}{\Omega_1 \Gamma_B} \quad \text{and} \quad \xi_2 = \frac{\Omega_B^2 - \Omega_2^2}{\Omega_2 \Gamma_B}. \quad (6)$$

L is the fiber length, P_1 is the CW power, P_{10} is the initial CW power, P_2 is the SW power, P_{20} is the initial SW power, P_3 is the ASW power, P_{30} is the initial ASW power, k is the CW vector modulus in vacuum, r is the radius of fiber, and $\omega = \omega_1 \approx \omega_2 \approx \omega_3$ and $q = q_1 \approx q_2$.

System (3) was solved numerically using the Scilab package from INRIA, making use of boundary conditions (4), to feature the power distribution of

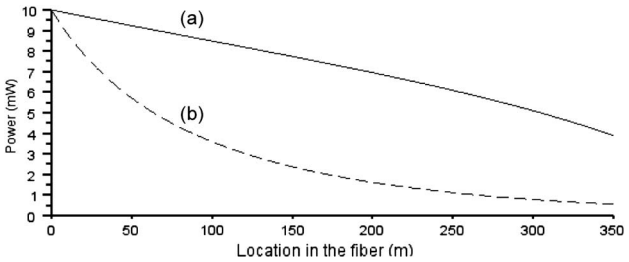

Fig. 2. ASW power distribution inside the optical fiber (a) gain *and* loss regime: $P_{20} = 10$ mW and (b) gain *or* loss regime: $P_{20} = 0$ mW $n = 1.48$, $\gamma_e = 0.902$, $\lambda = 1550$ nm, $\rho_0 = 2.21$ g/cm^3, $v = 5616$ m/s, $\Gamma_B = 0.1$ GHz, $\alpha = 0.2$ dB/km, $L = 350$ m, $P_{10} = 10$ mW, $P_{30} = 10$ mW.

the ASW inside the optical fiber, for given input CW and SW powers. A typical power distribution of the ASW is shown in Fig. 2 for the case of (a) combined Brillouin gain and loss, for which all three initial powers are 10 mW and (b) Brillouin gain or loss, where the Stokes input power has been set to "0." The goal of the study of these distributions is to show that the model described in system (3) does, indeed, describe the combined Brillouin gain and loss process, depicted by the solid line, which shows significant depletion reduction as compared with the Brillouin gain or loss processes, depicted by the dashed line. The parameters used for the simulations in this paper are shown in Table 1 below.

The NAND gate has been characterized by its truth table, where "0" and "1" are logical values of the truth table. For the current study, a power of 0.1 mW was assigned a logical value of "0," while a power of 10 mW was assigned a logical value of "1." Several configurations, depending on P_{30} and the availability of detuning have been considered. P_{10} and P_{20} are used as input signals, P_{30} is used as the reference signal, and the output ASW power, $P_{3\text{-out}}$, is used as the output signal of the NAND gate.

3. Results and Discussion

A. NAND Gate

It has been determined that obtaining a logical output of exactly 0.1 or 10 mW is not feasible. However, it is possible to obtain output signals within a given level of tolerance. In this manuscript, a threshold value of at least 20% is deemed acceptable. Switching contrast bar graphs are introduced in Figs. 3, 4, 6, and 9, showing the output signals as percentages of the optimal signal power of 10 mW. The tolerance between the low and high thresholds is the resultant switching contrast of the logic gate configuration. The higher the switching contrast, the more accurate the logical "0" and "1" representation is by the real circuit.

Table 1. Simulation Parameters

Index of refraction n	1.48
Electrostrictive constant γ_e	0.902
Wavelength of pump laser λ	1550 nm
Density of fiber ρ_0	2.21 g/cm^3
Speed of sound v	5616 m/s
Brillouin linewidth Γ_B	0.1 GHz
Fiber attenuation α	0.2 dB/km
Power penalty	0.67 dB/km

1. *Configuration I*

In configuration I, a fiber length of $L = 2300$ m was used (shorter fiber length is possible with lower switching contrast), and the ASW reference signal was kept constant at $P_{30} = 40$ mW. The logical output "1" corresponds to several different values of output power, namely 25.1, 25.0, and 7.48 mW for the logical inputs "0 0," "0 1," and "1 0," respectively, while the logical output "0" corresponds to an output ASW power of 5.47 mW.

As can be seen from Fig. 3(a), configuration I has a switching contrast of 20.6%, which could be acceptable. It is technologically the easiest to implement, since all signals are in resonance, and no frequency detuning is required.

If a higher switching contrast is desired, amplitude modulation of the P_{30} input ASW power is introduced, arriving to configuration II.

2. *Configuration II*

Configuration II is characterized by a slightly shorter fiber length of $L = 500$ m, as well as an amplitude modulation of the input ASW power for various inputs. Namely, for the "0 0," "0 1," and "1 1," inputs, $P_{30} = 10$ mW, while for the "1 0" input, $P_{30} = 40$ mW. As a result, output powers of 8.80, 8.78, 10.9, and 3.58 mW were obtained for the logical inputs "0 0," "0 1," "1 0," and "1 1," respectively.

As can be seen from Fig. 3(b), configuration II has an increased switching contrast of 52.7%. The tradeoff is the required change in ASW input power for the "1 0" logical input. As such, some additional calibrations would be needed to realize the function of this logic gate, since it would require amplitude switching of the reference ASW signal, making it more difficult to implement than configuration I.

To further optimize the switching contrast, detuning of the SW or ASW signals has been introduced instead of amplitude modulation of the P_{30} signal in configuration III.

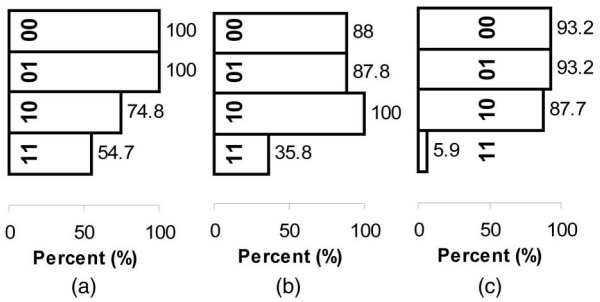

Fig. 3. NAND gate switching contrast plots (a) configuration I: low threshold: 54.7%, high threshold: 74.8%, tolerance: 20.6%. (b) Configuration II: low threshold: 35.8%, high threshold: 87.8%, tolerance: 52.7%. (c) Configuration III: low threshold: 5.9%, high threshold: 87.7%, tolerance: 82.8%.

3. *Configuration III*

Figure 10 depicts the output ASW power spectra for typical NAND gate inputs. From Fig. 10, it can be seen that it is possible to optimize the output signal via detuning of either the SW or ASW signals. For each input "0 0," "0 1," "1 0," and "1 1," a detuning greater than $\pm 3\Gamma_B$ is sufficient to obtain a maximum switching contrast within 2%–3%.

Configuration II utilizes a fiber length of $L = 350$ m, as well as detuning of the SW and ASW to achieve a maximum switching contrast. Namely, for the "0 0," "0 1," and "1 0" inputs, the ASW is detuned by $\pm 3\Gamma_B$, while for the "1 1" input, the SW is detuned by $\pm 3\Gamma_B$. As a result, output powers of 9.32, 9.32, 8.77, and 0.59 mW were obtained for the logical inputs "0 0," "0 1," "1 0," and "1 1," respectively. In this configuration, the reference ASW signal was held constant at $P_{30} = 10$ mW.

Configuration III requires a tunable laser source, capable of detuning the SW and ASW separately. Although technologically this is more complicated to realize, the tunable frequency range is very large and, in this case, any detuning outside $\pm 3\Gamma_B$ (about ± 0.3 GHz) will provide the maximum switching contrast of 82.8%, within 2%–3%. As such, this configuration also benefits from a shorter fiber length of 350 m, which acts to compactify the setup.

B. NOT Gate

1. *Configuration IV*

Although, according to DeMorgan's theorem [37], any logic gate may be constructed from several NAND gates, practical considerations may require a simplified design of certain simple gates, such as the NOT, AND, etc. In view of this, the design for an all-optical NOT gate was considered, using a similar approach as for the NAND gate described in previous sections. The combination of the NAND and NOT gates may be used to create a simplified AND gate, which would require minimal calibration and yield a high switching contrast.

In configuration IV, the initial CW power, P_{10}, was chosen to be the input signal, and the output ASW power, $P_{3\text{-out}}$, was taken to be the output signal of the optical gate. In this case, the input SW is a reference signal, and was held constant at $P_{20} = 10$ mW.

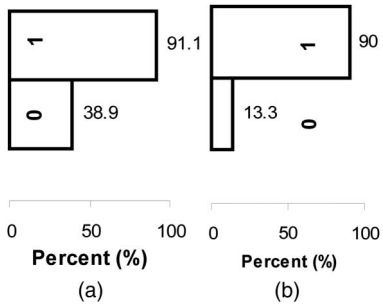

Fig. 4. NOT gate switching contrast plots (a) configuration IV: low threshold: 38.9%, high threshold: 91.1%, tolerance: 52.9%. (b) Configuration V: low threshold: 13.3%, high threshold: 90.0%, tolerance: 77.6%.

As before, a power of 0.1 mW was assigned a logical value of "0," while a power of 10 mW was assigned a logical value of "1." Output powers of 9.11 and 3.89 mW were obtained for the logical inputs "0" and "1," respectively. In this configuration, a fiber length of $L = 350$ m was used.

The proposed configuration of the NOT gate has all the technological benefits of the NAND gate in configuration I, as well as a switching contrast of 52.9%, as can be seen from Figure 4(a).

2. *Configuration V*

Another possible realization of the NOT gate utilizes the two-wave configuration of Brillouin gain. In this case, the initial SW power, P_{20}, was chosen to be the input signal, and the output CW power, $P_{1\text{-out}}$, was taken to be the output signal of the optical gate. The input CW was taken to be the reference signal, and was held constant at $P_{10} = 10$ mW. A power of 0.1 mW was assigned a logical value of "0," while a power of 10 mW was assigned a logical value of "1." Output powers of 9.0 and 1.33 mW were obtained for the logical inputs "0" and "1," respectively. In this configuration, a fiber length of $L = 350$ m was used.

As seen in Fig. 4(b), the proposed configuration of the NOT gate has a higher switching contrast of 77.6%, as compared to configuration IV. Additionally, the current NOT gate, based on the two-wave SBS interaction is substantially simpler in design, requiring the use of only two optical waves, as compared to three optical waves.

C. AND Gate

1. *Configuration VI*

In the current configuration, an AND gate is constructed by connecting the NAND gate of configuration III with the NOT gate of configuration IV, shown schematically in Fig. 5 below.

P_{10} and P_{20}, represented by CW_1 and SW_1 in Fig. 5 above, are the input signals of the AND gate, while the initial power of the reference signal ASW_1 is held constant at $P_{30} = 10$ mW. The output ASW'_1 signal from the NAND gate, $P_{3\text{-out}}$, is frequency downshifted from ω_3 to ω_1, turning it into an effective CW_2 wave, which is the input signal for the NOT gate. SW_2 and ASW_2 are the reference signals of the NOT gate, and are kept constant at 10 mW. The output signal of the AND gate is the ASW'_2 signal. As before, a power of 0.1 mW was assigned a logical value of "0," while a power of 10 mW was assigned a logical value of "1." Output powers of 4.02, 4.02, 4.14, and 8.31 mW were obtained for the logical inputs "0 0," "0 1," "1 0," and "1 1," respectively. In this configuration, a fiber length of

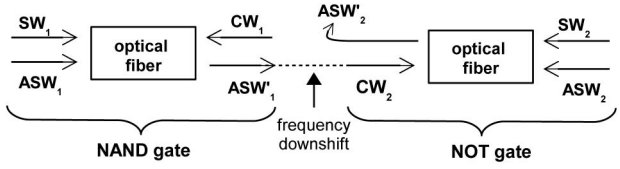

Fig. 5. Schematic of configuration VI: AND gate.

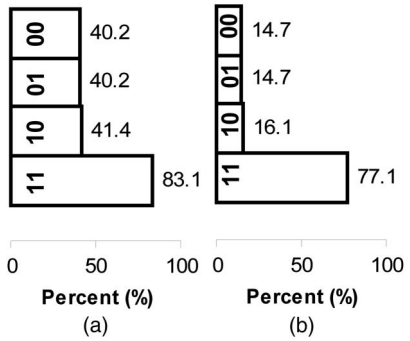

Fig. 6. AND gate switching contrast plots (a) configuration VI: low threshold: 40.2%, high threshold: 83.1%, tolerance: 42.3%. (b) Configuration VII: low threshold: 16.1%, high threshold: 77.1%, tolerance: 61.8%.

$L = 350$ m was used for both the NAND gate and NOT gate.

The same detuning must be applied to optical signals entering the NAND gate as stated in the description of configuration III. For the subsequent NOT gate, input signals should be kept at resonance.

As can be seen from Fig. 6(a), configuration VI of the AND gate yields a switching contrast of 42.3%.

2. *Configuration VII*

In the current configuration, an AND gate is constructed by connecting the NAND gate of configuration III with the NOT gate of configuration V, shown schematically in Fig. 7 below.

Similar to configuration VI, P_{10} and P_{20}, represented by CW_1 and SW_1 in Fig. 7 above, are the input signals of the AND gate, while the initial power of the reference signal ASW_1 is held constant at $P_{30} = 10$ mW. The output ASW'_1 signal from the NAND gate, $P_{3\text{-out}}$, is frequency downshifted from ω_3 to ω_2, turning it into an effective SW_2 wave, which is the input signal for the NOT gate. The reference signal CW_2 is kept constant at 10 mW. The output signal of the AND gate is the CW'_2 signal. As usual, a power of 0.1 mW was assigned a logical value of "0," while a power of 10 mW was assigned a logical value of "1." Output powers of 1.47, 1.47, 1.61, and 7.71 mW were obtained for the logical inputs "0 0," "0 1," "1 0," and "1 1," respectively. Once again, a fiber length of $L = 350$ m was used for both the NAND gate and NOT gate.

The same detuning must be applied to optical signals entering the NAND gate as stated in the description of configuration III. For the subsequent NOT gate, input signals should be kept at resonance.

As can be seen from Fig. 6(b), configuration VI of the AND gate yields a switching contrast of 61.8%. This is higher than the switching contrast on configuration VI; additionally, the setup is substantially simpler since the NOT gate from configuration V requires a two-wave SBS interaction.

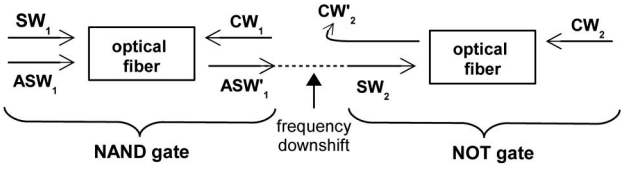

Fig. 7. Schematic of configuration VII: AND gate.

D. Configuration VIII

In another possible configuration, loops mirrors [38] and high-order mode fibers (HOM) [39,40] are utilized to reuse the fiber under test. Loops mirrors redirect output light back into a different mode of the HOM, thereby compactifying the setup. In this configuration, only one fiber, which must be an HOM fiber, is required. Since HOM fibers do not maintain the polarization of propagating light, this configuration is more prone to polarization instabilities and PMD. Another possibility is to use a PMF, whereby loop mirrors redirect output light back into a perpendicularly polarized state in the same fiber, similar to the implemented schemes in [41,42]. This would also act to compactify the setup while helping to eliminate the influence of polarization instability and PMD.

E. OR Gate

1. *Configuration IX*

To create a functional OR gate, three NAND gates from configuration III must be connected, shown schematically in Fig. 8 below.

CW_1 and SW_1, as well as CW_2 and SW_2 in Fig. 8 above, are the input signals of the OR gate. CW_1 and SW_1, and CW_2 and SW_2, must always have identical power. The initial power of the reference signals ASW_1 and ASW_2 is held constant at 10 mW. The output ASW'_1 signal from NAND gate 1 is frequency downshifted from ω_3 to ω_1, turning it into an effective CW_3 wave, which is an input signal for the NAND gate 3. The output ASW'_2 signal from NAND gate

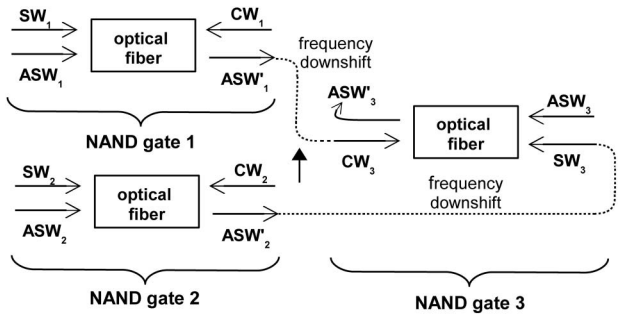

Fig. 8. Schematic of configuration IX: OR gate.

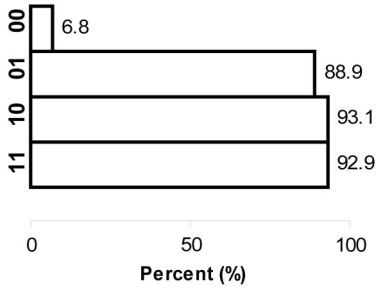

Fig. 9. OR gate switching contrast plot low threshold: 6.8%, high threshold: 88.9%, tolerance: 83.0%.

2 is frequency downshifted from ω_3 to ω_2, turning it into an effective SW_3 wave, which is another input signal for the NAND gate 3. The reference signal of NAND gate 3, ASW_3, is held constant at 10 mW. The output signal of the OR gate is the ASW_3' signal. A power of 0.1 mW was assigned a logical value of "0," while a power of 10 mW was assigned a logical value of "1." Output powers of 0.64, 8.78, 9.29, and 9.29 mW were obtained for the logical inputs "0 0," "0 1," "1 0," and "1 1," respectively. A fiber length of $L = 350$ m was used for all three NAND gates.

The same detuning must be applied to optical signals entering all three NAND gates as stated in the description of configuration III.

As can be seen from Fig. 9, configuration IX of the OR gate yields a switching contrast of 83.0%. Though the current configuration is more complicated than the previous ones, it also yields an extremely high switching contrast.

4. Conclusion

A fiber nonlinearity-based technique has been proposed to realize all-optical NAND/NOT/AND/OR logic gates, based on the principles of combined Brillouin gain and loss in a PMF. Switching contrasts are simulated to be between 20% and 83%, for various configurations. In addition, the technique is not limited by polarization instabilities or PMD.

The authors acknowledge the financial support of the University of Ottawa and CREATE, and the NSERC discovery grant.

Appendix A:

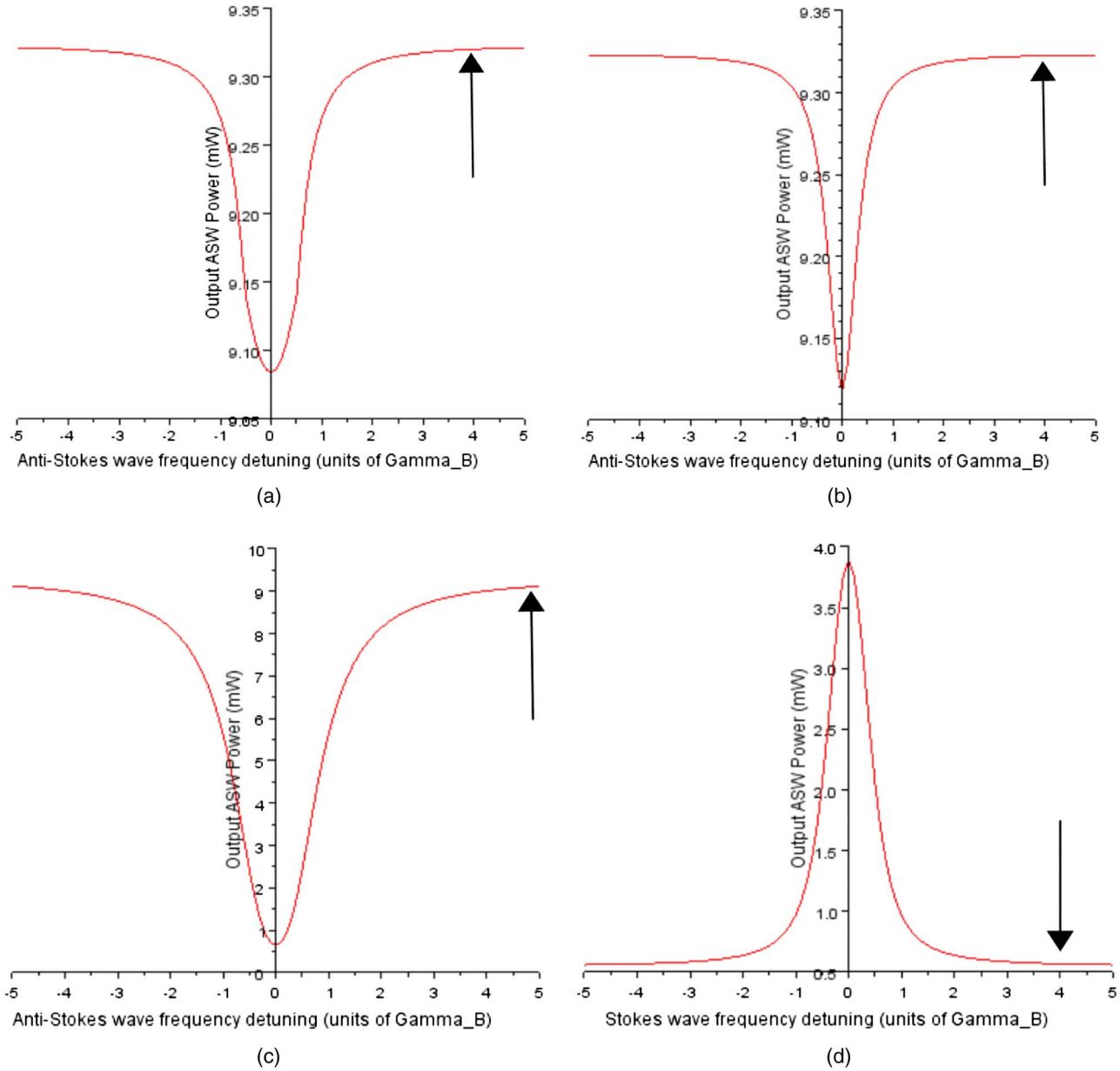

Fig. 10. Output ASW power spectra (a) "0 0" input, (b) "0 1" input, (c) "1 0" input, and (d) "1 1" input.

References

1. T. Chattopadhyay, "Optical programmable Boolean logic unit," Appl. Opt. **50**, 6049–6056 (2011).
2. T. Chattopadhyay, "Optical reversible programmable Boolean logic unit," Appl. Opt. **51**, 5266–5271 (2012).
3. M. R. Fetterman, "Design for high-speed optoelectronic Boolean logic," IEEE Photon. Technol. Lett. **21**, 1740–1742 (2009).
4. J. Yang, X. Li, J. Yang, J. Liu, and X. Su, "Polarization-independent bidirectional 4 × 4 optical switch in free-space," Opt. Laser Technol. **43**, 927–933 (2010).
5. Y. Wu, T. Shih, and M. Chen, "New all-optical logic gates based on the local nonlinear Mach–Zehnder interferometer," Opt. Express **16**, 248–257 (2008).
6. M. Nazari and M. Haghparast, "Novel design of all-optical reversible logic gate using Mach–Zehnder interferometer in the field of nanotechnology," Australian J. Basic Appl. Sci. **5**, 923–929 (2011).
7. T. Chattopadhyay, "All-optical modified Fredkin gate," IEEE J. Sel. Top. Quantum Electron. **18**, 585–592 (2012).
8. Z. Li and G. Li, "Ultrahigh speed reconfigurable logic gates based on four-wave mixing in a semiconductor optical amplifier," Photon. Tech. Lett. **18**, 1341–1343 (2006).
9. S. H. Kim, J. H. Kim, B. G. Yu, Y. T. Byun, Y. M. Jeon, S. Lee, D. H. Woo, and S. H. Kim, "All-optical NAND gate using cross-gain modulation in semiconductor optical amplifiers," Electron. Lett. **41**, 1027–1028 (2005).
10. D. Nesset, T. Kelly, and D. Marcenac, "All-optical wavelength conversion using SOA nonlinearities," IEEE Commun. Mag. **36**, 56–61 (1998).
11. C. Schubert, R. Ludwig, and H.-G. Weber, "High-speed optical signal processing using semiconductor optical amplifiers," J. Opt. Fiber Comm. Reports **2**, 171–208 (2004).
12. X. Ye, P. Ye, and M. Zhang, "All-optical NAND gate using integrated SOA-based Mach–Zehnder interferometer," Opt. Fiber Technol. **12**, 312–316 (2006).
13. T. Chattopadhyay, "All-optical programmable Boolean logic unit using SOA-MZI switch," IET Optoelectronics **5**, 270–280 (2011).
14. K. I. Kang, T. G. Chang, I. Glesk, and P. R. Prucnal, "Comparison of Sagnac and Mach–Zehnder ultrafast all-optical interferometric switches based on semiconductor resonant optical nonlinearity," Appl. Opt. **35**, 417–426 (1996).
15. J. Y. Kim, J. M. Kang, T. Y. Kim, and S. K. Han, "All-optical multiple logic gates with XOR, NOR, OR, and NAND functions using parallel SOA-MZI structures: theory and experiment," J. Lightwave Technol. **24**, 3392–3399 (2006).
16. J. Wang, J. Sun, and Q. Sun, "Experimental observation of a 1.5 μm band wavelength conversion and logic NOT gate at 40 Gbit/s based on sum-frequency generation," Opt. Lett. **31**, 1711–1713 (2006).
17. J. Wang, J. Sun, and Q. Sun, "Proposal for all-optical switchable OR/XOR logic gates using sum-frequency generation," IEEE Photon. Technol. Lett. **19**, 541–543 (2007).
18. Z. Y. Shen and L. L. Wu, "Reconfigurable optical logic unit with terahertz optical asymmetric demultiplexer and electro-optic switches," Appl. Opt. **47**, 3737–3742 (2008).
19. T. Chattopadhyay, "Eliminating the additional input beam in all-optical XOR gate using terahertz optical asymmetric demultiplexer (TOAD) based interferometer: a theoretical analysis," Optik International J. Light Electron. Opt. **122**, 1486–1491 (2011).
20. T. Chattopadhyay, "All-optical terahertz optical asymmetric demultiplexer (TOAD) based binary comparator: a proposal," J. Nonlinear Opt. Phys. Mater. **18**, 471–480 (2009).
21. T. Chattopadhyay, "All-optical cross-bar network architecture using TOAD based interferometric switch and using it to design reconfigurable logic unit," Opt. Fiber Technol. **17**, 558–567 (2011).
22. A. W. Lohmann, "Polarization and optical logic," Appl. Opt. **25**, 1594–1597 (1986).
23. M. A. Karim, A. A. S. Awwal, and A. K. Cherri, "Polarization-encoded optical shadow-casting logic units: design," Appl. Opt. **26**, 2720–2725 (1987).
24. T. Chattopadhyay and T. Sarkar, "All-optical by Kerr nonlinear prism and its application to of binary-to-gray-to-binary code conversion," Opt. Laser Technol. **44**, 1722–1728 (2012).
25. C. Yu, L. Christen, T. Luo, Y. Wang, Z. Pan, L. Yan, and A. E. Willner, "All-optical XOR gate using polarization rotation in single highly nonlinear fiber," Photon. Tech. Lett. **17**, 1232–1234 (2005).
26. C. Yu, L. Christen, T. Luo, Y. Wang, Z. Pan, L. Yan, and A. E. Willner, "All-optical XOR gate based on Kerr effect in single highly-nonlinear fiber," Proc. Conf. Lasers Electro-Optics (2004), pp. 3–5.
27. K. Suzuki, H. Kubota, S. Kawanishi, M. Tanaka, and M. Fujita, "Optical properties of low-loss polarization-maintaining photonic crystal fiber," Opt. Express **9**, 676–680 (2001).
28. T. Hosaka, K. Okamoto, T. Miya, Y. Sasaki, and T. Edahiro, "Low-loss single polarization fibers with asymmetrical strain birefringence," Electron. Lett. **17**, 530–531 (1981).
29. R. D. Birch, D. N. Payne, and M. P. Varnham, "Fabrication of polarization-maintaining fibers using gas-phase etching," Electron. Lett. **18**, 1036–1038 (1982).
30. W. Zou, C. Jin, and J. Chen, "Distributed strain sensing based on combination of Brillouin gain and loss effects in Brillouin optical correlation domain analysis," Appl. Phys. Express **5**, 082503 (2012).
31. K. Y. Song, Z. He, and K. Hotate, "Distributed strain measurement with millimeter-order spatial resolution based on Brillouin optical correlation domain analysis," Opt. Lett. **31**, 2526–2528 (2006).
32. W. Zou, Z. He, M. Kishi, and K. Hotate, "Stimulated Brillouin scattering and its dependences on strain and temperature in a high-delta optical fiber with F-doped depressed inner cladding," Opt. Lett. **32**, 600–602 (2007).
33. X. Bao and L. Chen, "Recent progress in Brillouin scattering based fiber sensors," Sensors **11**, 4152–4187 (2011).
34. R. Boyd, *Nonlinear Optics* (Academic, 1992).
35. L. Chen and X. Bao, "Analytical and numerical solutions for steady state stimulated Brillouin scattering in a single-mode fiber," Opt. Commun. **152**, 65–70 (1998).
36. Y. Li, X. Bao, Y. Dong, and L. Chen, "A novel distributed Brillouin sensor based on optical differential parametric amplification," J. Lightwave Technol. **28**, 2621–2626 (2010).
37. A. Kumar, *Switching Theory and Logic Design* (PHI Learning Private Limited, 2008).
38. N. J. Doran and D. Wood, "Nonlinear-optical loop mirror," Opt. Lett. **13**, 56–58 (1988).
39. S. H. Larsen, M. E. V. Pedersen, L. Gruner-Nielsen, M. F. Yan, E. M. Monberg, P. W. Wisk, and K. Rottwitt, "Polarization maintaining higher order mode fiber module with anomalous dispersion at 1 μm," Opt. Lett. **37**, 4170–4172 (2012).
40. M. Tur, E. Herman, A. Kozhekin, and Y. Danziger, "Stimulated Brillouin scattering in high-order mode fibers employed in dispersion management modules," IEEE Photon. Technol. Lett. **14**, 1282–1284 (2002).
41. A. Bogoni, L. Poti, R. Proietti, G. Meloni, F. Ponzini, and P. Ghelfi, "Regenerative and reconfigurable all-optical logic gates for ultra-fast applications," Electron. Lett. **41**, 435–436 (2005).
42. Y. Miyoshi, R. Ikeda, H. Tobioka, T. Inoue, S. Namiki, and K. Kitayama, "Ultrafast all-optical logic gate using a nonlinear optical loop mirror based multi-periodic transfer function," Opt. Express **16**, 2570–2577 (2008).